Journal of Cultural Heritage 52 (2021) 146–152

Contents lists available at ScienceDirect

Journal of Cultural Heritage

journal homepage: www.elsevier.com/locate/culher

Case Study

Exploring the chemical composition and corrosion patterns of arrowheads used in the Siege of Motya (397 BC) through a multi-analytical approach

Martina Bernabale[a], Lorenzo Nigro[b], Daria Montanari[b], Caterina De Vito[a,*]

[a] Department of Earth Sciences, Sapienza University of Rome, P.le Aldo Moro 5, 00185 Rome, Italy
[b] Department Italian Institute of OrientalStudies - ISO, Sapienza University of Rome, Circonvallazione Tiburtina 4, 00185, Rome, Italy

ARTICLE INFO

Article history:
Received 18 March 2021
Accepted 1 October 2021
Available online 16 October 2021

Keywords:
Arrowheads
SEM-EMPA-XRPD
Copper alloys
Copper trihydroxychlorides
Corrosion stratigraphy
Lead globules corrosion

ABSTRACT

This study examines a set of bronze arrowheads involved in the Siege of Motya (Italy) and aims to determine their microstructures, corrosion patterns and production techniques using Scanning Electron Microscope, X-ray maps, Electron Microprobe Analysis and X-ray diffraction. The arrowheads characterized by plane and conical shapes are made from Cu-Sn-alloy, featuring Liesegang rings with streaks of Sn-oxide interposed between Cu_2O and $Cu_2(OH)_3Cl$ layers. Those of pyramidal or lanceolate shapes are made from Cu-Pb-Sn alloy and contain different corrosive products triggered by exposure to high levels of chloride-rich conditions. These results have highlighted an interesting correlation between alloy microstructures, compositions, typology and geographic provenance, and thus provide new insight on the weaponry and poliorcetics of the Syracusan army that led to the defeat of Motya in 397/6 BC.

Introduction

Metallic materials return to their primitive mineral state due to corrosion processes [35] involving reactions that are driven by corrosive agents or contaminants and microstructural constraints [10, 13, 15, 36]. The corrosion rate of bronze and the formation of patina are particularly influenced by chlorine content in the environment, resulting in higher corrosion rates and thicker patinas in chloride-rich marine settings [4, 5, 32].

Ancient copper-based alloys display complex microstructures of corrosion, which have been classified by Robbiola et al. [31] into two main types. Type I (even surfaces) is characterized by excellent corrosion-resistant properties; it consists primarily of a bi-layer that grows on the original surface facing the alloy, without any apparent change of volume. Type II structures (coarse surfaces) are characterized by the presence of high amounts of chloride on the internal layer or alloy interface, with localized corrosion phenomena or more generalized attacks due to the high dissolution rate of metal. Based on Robbiola's classification (1998), a study by Constantinides et al. [8] has classified five different copper alloys of artificial patina layers. These results have shown that the Type I structure is characteristic of quaternary bronze and brass, Type II is typical of arsenical copper and tin bronze, and the presence of both structures can be found in leaded bronze [8].

Moreover, bronze artefacts may also be characterized by complex patterns of stratified and reoccurring corroded layers, the so-called "Liesegang Effect" [29, 35, 34,37,38]. Liesegang rings are formed by the periodic precipitation of products in heterogeneous liquid-solid systems; they are dispersed zonally or radially, continuously or interrupted by deep cracks [36, 38,34]. This type of corrosion is characterized by the accumulation of metastable cuprous chlorides that form close to the substrate.

The present study contributes to the investigation of corrosion processes on copper-based artefacts using a multi-analytical approach that includes Scanning Electron Microscope, X-ray maps, Electron Microprobe Analysis and X-ray Powder Diffraction.

To better understand manufacturing and corrosion processes, cross-sections of nine arrowheads are analysed "from rim-core-to-rim" (see also [2, 10, 11, 13, 28]). The opportunity to conduct invasive sampling is not common in the field of Cultural Heritage due to the limitations of the samples and the unique nature of the artefacts. However, this kind of approach is the only way to obtain a

* Corresponding author.
E-mail address: caterina.devito@uniroma1.it (C. De Vito).

https://doi.org/10.1016/j.culher.2021.10.001
1296-2074/

Table 1
Schematic classification and morphological features of the arrowheads.

Typology		Samples	Morphological Features	Geographical areas of attestation of types	Attribution
A.1 [42]		MM.78.151/8	Large arrowhead or javelin with lanceolate body, flat section and two barbs. Cold finishing with oblique and parallel streaks	Sicily, south-central Italy, Greece	Greeks
B.1 [42]		MD.17.8 MM.17.110	Small arrowheads with short triangular point, conical body, lateral wings, and short socket	Sicily, Tunisia, Spain, Sardinia, south-central Italy, Greece	Greeks/Phoenicians
'Scythian Type'	C.1 [42]	MM.16.162 MM.79.10 MD.17.114 MD.19.41	Short pyramidal arrowheads, with triangular or trefoil cross-section, and inner socket. Cold finishing	Sicily, Tunisia, Spain, central-southern Italy, Greece	Greeks
	C.2 [42]	MM.16.13	Short pyramidal arrowhead, with trefoil cross-section and short circular socket	Sicily, Tunisia, Spain, Sardinia, south-central Italy, Greece	Greeks/Phoenicians
D.1 [42]		MM.79.61	Conical arrowhead performed by wrapping a metal foil on itself overlapping edges	Sicily, Greece	Phoenicians

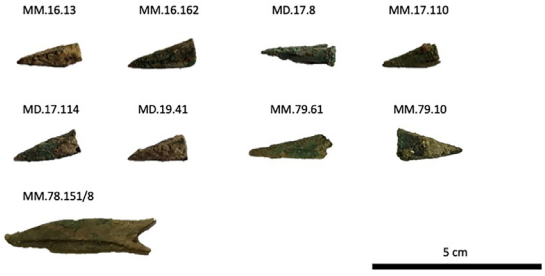

Fig. 1. Images of the bronze arrowheads studied in this work.

quantitative chemical analysis of the original alloys and to explore the corrosion process in more depth.

Archaeological context

The archaeological site of Motya, located at the centre of the Marsala Lagoon in Sicily, was one of the most important colonies in Phoenician-Punic Sicily and later became a strategic node for Carthaginian control over the Mediterranean.

In the early 4th century BC, Dionysius I the Tyrant, the dictator of the Greek city of Syracuse, attacked Motya with the intent to conquer central-western Sicily. As reported by Siculus et al. [40], the siege of Motya was important for the creation of innovative Greek artillery technology and military-industry under Dionysius I. The Phoenicians, although by nature a peaceful and non-warlike people, were skilled masters in the production of weapons. For several centuries they exported precious goods and apparatus objects to their Mediterranean colonies and counterparts.

Metallic arrowheads from Motya have revealed the manufacturing skills and knowledge of metalworkers in the Mediterranean during the 5th and 4th centuries BC; by studying their metallurgic features in depth, we are able to distinguish the arrowheads used by the aggressors from those of the losers, thus linking the properties of these metallic materials to historic battles and conflicts.

Research aims

In this study, a collection of bronze arrowheads (Fig. 1 and Table 1) from Motya were examined with three main goals in mind. First, the study aims to evaluate the role of alloy composition and manufacturing on the corrosion microstructures. Secondly, it explores the corrosion products formed in a saline coastal environment. The third and final challenge is to link the microstructures and alloy compositions of these artefacts to their morphological typologies and infer the mechanical properties of these weapons.

Materials and methods

Materials

Archaeological excavations at Motya, directed by Prof. Lorenzo Nigro of the University of Rome "La Sapienza" since 2002, have brought to light several types of arrowheads dating back to the siege of Dionysius, the Tyrant of Syracuse, who conquered the island in 397/6 BC [24, 26, 43].

Information on the samples, *i.e.,* typology, morphological features and geographical areas of attestation [42], is reported in Table 1.

Methods

Microstructure, qualitative and semi-quantitative chemical analyses were obtained using Scanning Electron Microscopy acquired with a FEI-Quanta 400 (SEM-EDS) instrument, equipped with X-ray energy-dispersive spectroscopy (Department of Earth Sciences, Sapienza University, Rome, Italy). SEM imaging was collected both in secondary electron (SE) and back scattered electron (BSE) modes. Energy-dispersive X-ray spectroscopy (EDS) spectra and X-ray maps were also used to show the distribution of elements through the samples.

Quantitative Electron Microprobe Analysis (EMPA) has been carried out using a Cameca SX50 electron microprobe equipped with five wavelength-dispersive spectrometers (CNR–IGAG, Rome, c/o Department of Earth Sciences, Sapienza University of Rome).

To determine the nature of crystalline compounds of the patina, X-ray Powder diffraction (XRPD) analysis was performed on a small amount of powdered patina from the artefacts, using a Bruker D8 FOCUS diffractometer (Department of Earth Sciences, Sapienza University, Rome, Italy).

Supplementary material provides more information about the operating conditions of all the technologies used here.

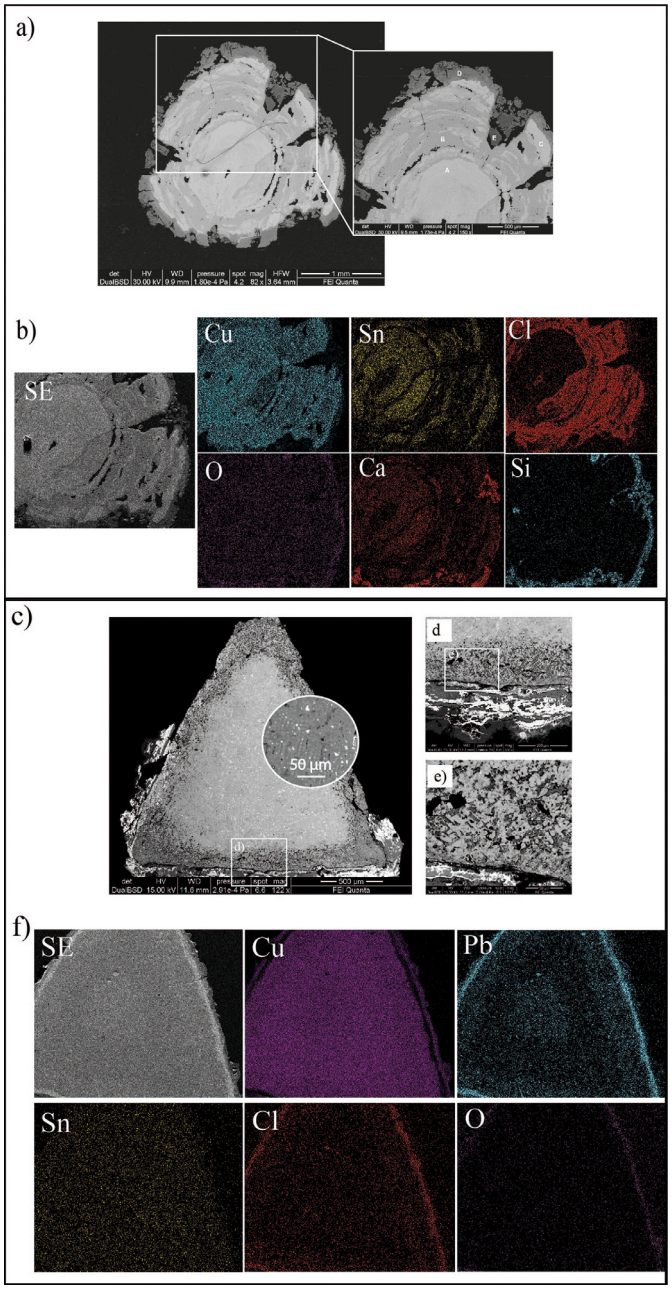

Fig. 2. BSE images of the sample MM.79.61 showing the microstructure at different magnification: 1 mm, 500 μm. Markers A, B, C, D, E correspond to corrosion layers reported in Fig. 4(a). Morphological image in SE and X-ray maps of sample MM. 79.61 (b). SEM-BSE cross sections of sample MM.16.162, showing type C.1 corrosive microstructure (c); details of the microstructure of the external corrosion layers composed by copper trihydroxichlorides (dark phase) and Pb chlorides (white phase) (d) and the enlarged view of layer A showing darker micro-domains enriched in Cu and Cl and lighter areas enriched in Cu, Sn and Cl (e). Morphological image in SE and X-ray maps of sample MM.79.10 (f).

Results and discussion

Alloy composition and microstructure through SEM- analysis and EMPA

The cross-section of sample MM.79.61 (Fig. 2a) highlights the presence of an inner core surrounded by concentric Liesegang rings. EDS and EMPA data of this sample (see Table 2) has revealed the presence of a copper-tin bronze alloy, where Cl, Si, Ca, Al and Mg are the main contaminants from the soil. Fig. 2a shows several corrosion layers in different shades of grey, including: 1) a white-grey phase in the core, defined by very high Cu content (*ca.* 88.99 wt%) with variable Sn content (8.33–16.72 wt%)(A); 2) a Cl-rich phase (up to 34.47 wt% Cl) occurring as grey bands, identified by a lower Cu (*ca.* 65.47 wt%) and Sn content (*ca.* 2.44 wt%) with respect to the previous layer (B); 3) the presence of a white-grey phase rich in Sn (*ca.* 8.13 wt%), demonstrating a similar chemical composition to the core of section C; and 4) Si- and Ca-rich phases in the darker layers (D, E). The strong variations of Cu, Sn and Cl content from one layer to another have also been confirmed by EMPA analysis on the different layers (Supplementary Fig. S2).

The distribution of each element has been analysed through X-ray mapping (Fig. 2b). Copper is the most abundant element, with the exception of the external areas affected by the dissolution of Cu *via* the decuprification mechanism [32]. The dissolved Cu reacts with soil anions such as chloride and then re-deposits in the next layer [29]. Tin occurs in alternating layers, forming Sn-rich and Sn-poor streaks. Generally, the content of Sn increases in conjunction with Cu dissolution, whereas it decreases in Cl-rich areas, similar to what has been reported by Hutchison and Scully [20]. Chlorine occurs in the dark-grey layers, where the dissolved Cu reacts with Cl and leads to the formation of copper trihydroxichlorides. The presence of oxygen in the outer and inner corroded layers suggests that the entire metallic structure has been oxidized.

Fig. 2b shows the presence of Ca and Si in the outermost corrosion layers due to the migration of these elements from the soil to the porous corrosion layers.

A possible explanation for the persistence of cuprous chloride (*e.g.* copper trihydroxychlorides) in the form of layered structures inside a mineralized bronze is reported by Organ [27]. These banded structures, known as the Liesegang Phenomena, could also be related to environmental changes in the burial environment. These types of corrosion microstructures have also been observed by Oudbashi et al. [29] in bronze artefacts from the Haft Tappeh Middle Elamite site (Iran) dating to the 14th century BC.

Samples MM.16.162, MM.79.10, MD.17.114 and MD.19.41 are trefoil arrowheads made of Cu-Sn-Pb ternary alloy with low Sn content (Table 2). As shown in Fig. 2c, Pb is distributed in the alloy as small particles that are immobilized throughout the matrix (*ca.* 94.87 wt% Cu, 3.99 wt% Sn), suggesting a higher cooling rate of the melt [19]. Sample MD.19.41 is the only exception as it displays bigger and round globules (Supplementary Fig. S1). In fact, the size of lead globules also depends on the amount of lead used and the post-casting manufacture. These low melting point inclusions are located along α-Cu-Sn grain boundaries due to the low miscibility of lead in copper, thereby making leaded bronzes more castable than binary bronzes [17, 44]. Indeed, lead is not involved in the formation of Cu and Sn alloys, but it occurs as islands in the matrix [3, 7, 22]. BSE images have revealed a multi-stratified corrosion structure. In this type of arrowhead (MM.16.162, MM.79.10, MD.17.114, MD.19.41) the inner corrosion layer of the arrowhead's edge is strongly depleted in Pb (*ca.* 11.05 wt%), whereas a micro-segregation of a Cu and Cl enriched phase has formed. Conversely, the external corrosion layers above the original surface consist of a darker layer of Cu (*ca.* 67.83 wt%) and Cl (*ca.* 30.90 wt%), attributed to the formation of copper trihydroxichlorides, and a brighter layer of Pb chlorides (*ca.* 50.84 wt%, Pb, 13.91 wt% Cl) (Fig. 2d,e).

The X-ray maps show that the content of Cu is distributed quite homogeneously in the matrix (Fig. 2f); however, as reported in Table 2, the Pb-rich patina (layer B) is entirely depleted in Cu due to the decuprification process (*ca.* 28.56 wt%) but enriched in the external layer (*ca.* 67.83 wt% in layer C). Fig. 2f also highlights a concentric distribution of Pb micro-domains in α-Cu–Sn homogeneous matrix, in which the darker layer has a lower amount of Pb. The distribution of Sn is homogeneous in the metal bulk. Finally,

Table 2
Maximum (Max.), minimum (Min.) and average (Avg.) Normalized EMPA analyses of different layers in 9 bronze arrowheads from Motya (wt%). .

Type	TYPE C.1														
Area	Layer A			Layer B			Layer C			Layer D	Matrix				
Element	Max.	Min.	Avg.	Max.	Min.	Avg.	Max.	Min.	Avg.	Avg.	Max.	Min.	Avg.		
Pb	13.96	6.60	11.05	71.36	22.05	50.84	0.81	0.34	0.56	12.77	1.94	0.09	0.54		
Cu	68.29	48.37	54.42	65.66	10.49	28.56	79.37	62.35	67.83	41.74	99.02	88.28	94.87		
As	0.64	0.23	0.50	0.33	0.01	0.15	n.d.	n.d.	n.d.	n.d.	0.32	0.01	0.16		
Sn	18.12	12.08	15.36	19.20	0.03	4.72	0.01	0.01	0.01	0.01	10.94	0.61	3.99		
Fe	0.73	0.21	0.48	8.83	0.04	1.58	0.07	0.02	0.05	2.67	0.31	0.01	0.16		
P	0.10	0.05	0.08	4.30	0.02	0.58	0.10	0.03	0.06	0.18	0.14	0.05	0.10		
Ca	0.04	n.d.	0.02	0.06	n.d.	0.03	0.05	0.01	0.03	0.20	0.05	n.d.	0.02		
Si	0.86	0.22	0.49	0.23	0.01	0.12	2.11	0.01	0.54	35.41	0.05	0.02	0.04		
S	0.45	0.04	0.18	0.06	n.d.	0.02	0.09	0.02	0.04	0.15	0.78	n.d.	0.30		
Ag	0.04	0.02	0.03	0.16	n.d.	0.04	0.08	0.03	0.05	n.d.	0.08	n.d.	0.03		
Cl	26.53	10.78	17.42	22.02	1.70	13.91	36.19	19.72	30.90	6.88	0.05	n.d.	0.02		
Type	TYPE D.1														
Area	Layer A1			Layer A2			Layer B			Layer C			Layer D		
Element	Max.	Min.	Avg.	Max.	Min.	Avg.	Max.	Min.	Avg.	Max.	Min.	Avg.	Max.	Min.	Avg.
Pb	0.06	n.d.	0.03	0.07	n.d.	0.03	0.04	0.01	0.03	0.05	n.d.	0.02	0.02	n.d.	0.01
Cu	98.20	57.74	88.99	84.23	59.02	67.43	69.62	57.74	65.47	92.08	87.80	89.44	89.02	12.04	50.53
As	0.85	n.d.	0.38	0.75	0.44	0.59	0.53	n.d.	0.09	0.48	0.17	0.28	n.d.	n.d.	n.d.
Sn	16.72	0.01	8.33	14.04	11.29	12.81	13.28	0.01	2.44	9.92	6.01	8.13	n.d.	n.d.	n.d.
Fe	1.24	n.d.	0.48	0.70	0.41	0.52	0.65	n.d.	0.13	0.71	0.33	0.45	4.91	1.39	3.15
P	n.d.	n.d.	n.d.	n.d.	n.d.	n.d.	n.d.	n.d.	n.d.	n.d.	n.d.	n.d.	n.d.	n.d.	n.d.
Ca	0.03	n.d.	0.01	0.06	n.d.	0.04	0.08	n.d.	0.04	0.07	n.d.	0.02	85.67	5.16	45.42
Si	n.d.	n.d.	n.d.	n.d.	n.d.	n.d.	n.d.	n.d.	n.d.	n.d.	n.d.	n.d.	n.d.	n.d.	n.d.
S	7.29	n.d.	1.24	0.09	0.05	0.07	0.14	n.d.	0.07	0.18	n.d.	0.08	0.62	0.33	0.48
Ag	0.12	n.d.	0.03	0.05	n.d.	0.03	0.03	n.d.	0.01	0.08	n.d.	0.03	0.07	0.02	0.05
Cl	0.92	0.09	0.43	28.27	0.31	18.37	34.47	27.44	31.66	3.05	0.67	1.45	0.44	0.08	0.26
Type	TYPE B.1-C.2												TYPE A.1		
Area	Matrix			Globules			ACI			Corrosion layer			Matrix		
Element	Max.	Min.	Avg.	Max.	Min.	Avg.	Max.	Min.	Avg.	Max.	Min.	Avg.	Max.	Min.	Avg.
Pb	13.29	0.41	5.01	98.73	62.88	82.25	15.27	12.27	13.77	83.63	11.44	56.80	0.66	0.15	0.31
Cu	97.00	79.80	90.34	12.70	0.03	3.44	81.93	78.81	80.37	76.52	0.61	25.13	98.84	94.72	96.33
As	0.50	0.05	0.20	0.04	n.d.	0.01	0.30	0.21	0.26	0.07	n.d.	0.01	0.33	0.07	0.21
Sn	9.35	2.02	5.55	9.52	n.d.	0.49	5.53	5.42	5.48	11.76	n.d.	3.89	3.79	0.62	2.68
Fe	0.05	n.d.	0.01	0.05	n.d.	0.01	0.01	n.d.	0.01	0.05	n.d.	0.01	0.07	0.01	0.03
P	0.12	0.03	0.09	0.06	n.d.	0.02	0.09	0.05	0.07	0.57	n.d.	0.10	n.d.	n.d.	n.d.
Ca	0.03	n.d.	0.01	0.05	n.d.	0.01	n.d.	n.d.	n.d.	0.85	n.d.	0.13	0.02	0.01	0.01
Si	0.46	0.01	0.07	0.03	n.d.	0.02	n.d.	n.d.	n.d.	8.00	n.d.	1.29	n.d.	n.d.	n.d.
S	0.17	n.d.	0.02	0.71	n.d.	0.09	0.02	0.02	0.02	0.99	n.d.	0.16	0.45	0.11	0.32
Ag	0.09	n.d.	0.04	1.76	n.d.	0.12	0.08	n.d.	0.04	0.09	n.d.	0.03	0.19	0.01	0.09
Cl	1.35	n.d.	0.12	23.47	0.11	13.53	n.d.	n.d.	n.d.	18.66	0.29	12.45	0.10	0.01	0.03

the presence of Cl and O in the patina can be justified as the main contaminants from the burial environment.

The arrowheads MM.16.13, MM.17.8 and MM.17.110 contain triangular sections consisting of a Cu-Sn matrix (*ca.* 98.84–94.72 wt% Cu and 3.79–0.62 wt% Sn) with large and irregular Pb-globules (Fig. 3a). This microstructure is comparable to a Sardinian bronze axe recovered in the excavations at Motya [2, 25]. These globules are heavily corroded (Fig. 3b) and, as demonstrated in Table 2, the concentration of chlorine varies from rim to core (0.1–23.5 wt% Cl). Another peculiar feature of this arrowhead typology is the presence of round structures inside the lead globules, which are visible in Fig. 3c. These metallic particles have a perfectly spherical shape, suggesting their origin is from a liquid phase. In fact, during casting Cu-Sn prills have been immobilized inside the lead globules due the poor mixing of copper and lead, which is the last phase to solidify in the system. The compositions of metallic prills are reported in Table 2 (80.4 wt% Cu, 13.8 wt% Pb and 5.5 wt% Sn). The content of Pb should derive from the area around the Cu-Sn globule. As suggested by Quaranta et al. [30], the formation of copper inclusions depends on thermodynamic equilibria, kinetic processes and solid-state diffusion processes. From a degradation point of view, these arrowheads (Types B.1 and C.2) show a very irregular and porous patina enriched in lead corrosion chlorides [2].

The X-ray maps in Fig. 3d show the cross-section distribution of alloy elements and soil contaminants. Cu and Sn are distributed uniformly in the matrix but are heavily depleted in the Pb-globules and patina due to the decuprification and destannification processes. The presence of chlorine in conjunction with oxygen and lead suggests the formation of insoluble lead oxidized products.

Arrowhead MM.78.151/8 is made of a Cu-Pb-Sn ternary alloy with a low amount of Sn. As shown in the BSE image, Pb occurs in the intergranular spaces throughout the stronger bronze matrix (*ca.* 96.33 wt% Cu and 2.68 wt% Sn) (Fig. 3e). The surface of this arrowhead is covered by a primary patina, which appears as a thin and brighter layer formed by Pb, surrounded by dark layers containing Cu and soil elements. The corrosion process takes the form of pitting or intergranular corrosion along grain boundaries or dendritic grain boundaries [1].

The X-ray maps in Fig. 3f show the distribution of Cu in the matrix, while Pb and Cl occur in the intergranular spaces and in the internal patina of the object, as chlorides, sulphates and carbonates. In the external layer, the presence of Cu in conjunction with O suggests the formation of cuprite in oxidized burial conditions. As a result of the decuprification process, the dissolved copper redeposits over the surface of the bronze. The presence of Ca in the outermost layer suggests the formation of copper and lead carbonates.

According to Robbiola's model, the corroded layers with chlorides in the inner layer/sound alloy interface of leaded bronze can be classified as Type II . The explanation for such corrosion can be found in the migration of chloride ions toward this interface, which

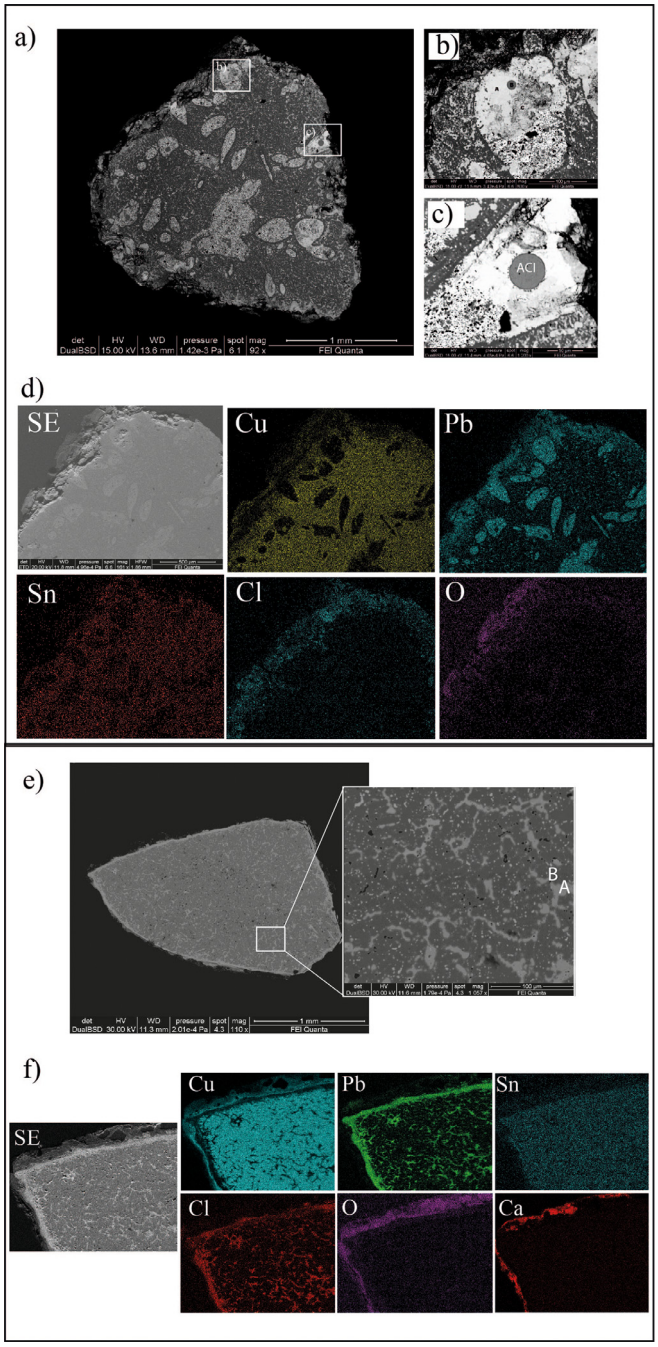

Fig. 3. SEM-BSE cross sections of sample MM.16.13, showing types B.1 and C.2 corrosive microstructure (a) with details of corroded Pb-globules with different concentration of chlorine (b) and spherical alloyed copper inclusion (c). Morphological image in SE and X-ray maps of sample MM.16.13 (d). BSE images of the sample MM.78.151/8 at different magnification: 1 mm, 100 μm Markers A and B represent the Pb-rich microdomains and the Cu-Sn matrix, respectively. (e). Morphological image in SE and X-ray maps of sample MM. 78.151/8 (f).

is connected to the incorporation of chloride anions into the oxygen vacancies of the lattice of corrosion products.

The chemical compositions of the nine arrowheads, acquired through EMPA, are reported in Table 2.

Characterization of corrosion products through XRPD- Analysis

Corrosion products were analysed using XRPD analysis (Supplementary Fig. S3,4,5,6,7); the results have revealed that the common elements affecting Motyan arrowheads are cuprite (Cu_2O) and atacamite ($Cu_2(OH)_3Cl$), which are commonly found on bronze artefacts buried in marine environments [16]. Quartz (SiO_2) occurs as a contaminant mineral deriving from the soil. The presence of both trihydroxichlorides (*i.e.*, atacamite and clinoatacamite) as corrosion products in arrowhead MM.79.61 seems to suggest a change in the ratio of hydroxyl/chloride in the solution [12]. Although nantokite (CuCl) has not been detected, it probably acted as a precursor to the formation of atacamite or paratacamite [9], causing the cyclic and inexorable reactions of oxidation and hydrolysis [46]. Aside from copper compounds, cassiterite (SnO_2) was detected only in sample MM.79.61. Tin seems to have had a positive impact in urban sites, whereas in marine environments it forms thicker and poorly adherent patinas [4]. Indeed, the presence of Sn in a chlorine-rich environment increases the corrosion rate of bronze artefacts compared to Cu metal, and it leads to the formation of $Cu_2(OH)_3Cl$ through redox reactions between intermediate Sn- and Cu-chlorides [5]. Sn-chlorides were not detected in the samples from Motya; this is probably due to the transitory nature of these compounds, which form soluble complexes that transform into SnO and/or SnO_2 [5].

Mixed salts of Cu and Pb, especially chlorides such as pseudoboleite ($Pb_5Cu_4Cl_{10}(OH)_8 \bullet 2(H_2O)$, occur in Type A.1 and C.1 arrowheads, whereas Pb-chlorides such as penfieldite ($Pb_2Cl_3(OH)$) and cotunnite ($PbCl_2$) appear in Type B.1 arrowheads. In particular, penfieldite occurs as a corrosion product in leaded-bronze objects buried in marine environments, *e.g.*, the Roman anchor recovered from the Mediterranean Sea [14, 18]. Instead, cotunnite surfaces as a marine corrosion product of Pb in acidic environments, where high chloride activities occur [14, 21].

According to Charlton et al. [6], Constantinides et al. [8], and Serghini-idrissi et al. [39], Pb-chlorides usually occur at grain boundaries as a consequence of selective dissolution of Pb in leaded bronze. In fact, a large amount of Pb migrates to the surface thorough the porosity of the alloy and then reacts with water, oxygen and chloride ions from the environment [30, 45].

The presence of cerussite ($PbCO_3$) relates to an increase of pH; this is due to oxygen reduction involving carbonate formation [39,41].

The green corrosion products are mainly copper (II) compounds such as malachite and atacamite [23], combined with silica and calcite from the soil.

Archaeological implications

Fig. 4 provides a schematic representation of each type of arrowhead, highlighting the main differences that occur in their microstructures and corrosive products.

EDS and EMPA results have revealed that the arrowheads with more accessory elements (such as wings and barbs) are of leaded-bronze and contain Pb-globules of different sizes. These pyramidal and lanceolate arrowheads (*i.e.*, Types A.1, B.1, C.1, C.2) have been attributed to the troops of Dionysius I of Syracuse by Termini [42] due to their frequency of attestation on the enemy battlefield (Motya). The addition of Pb reduces the melting point and simultaneously increases the fluidity of the melt, density and machinability of the alloy, resulting in an arrowhead that is more suitable for the production of complex objects that do not require high mechanical resistance. More specifically, the presence of Pb involves a gradual reduction of tensile strength, elongation, hardness, resistance to wear and deformation [33, 47]. It is worth noting that all of these arrowhead typologies have been recovered in multiple contexts in Greece, central-southern Italy, Tunisia, and Spain; in Sardinia, meanwhile, only Types B.1 and C.2 (bronze with high Pb content) have been recovered. This microstructure has also been observed in a Sardinian axe from Motya [2, 25], which suggests that Types B.1 and C.2, although known and used by the Greeks,

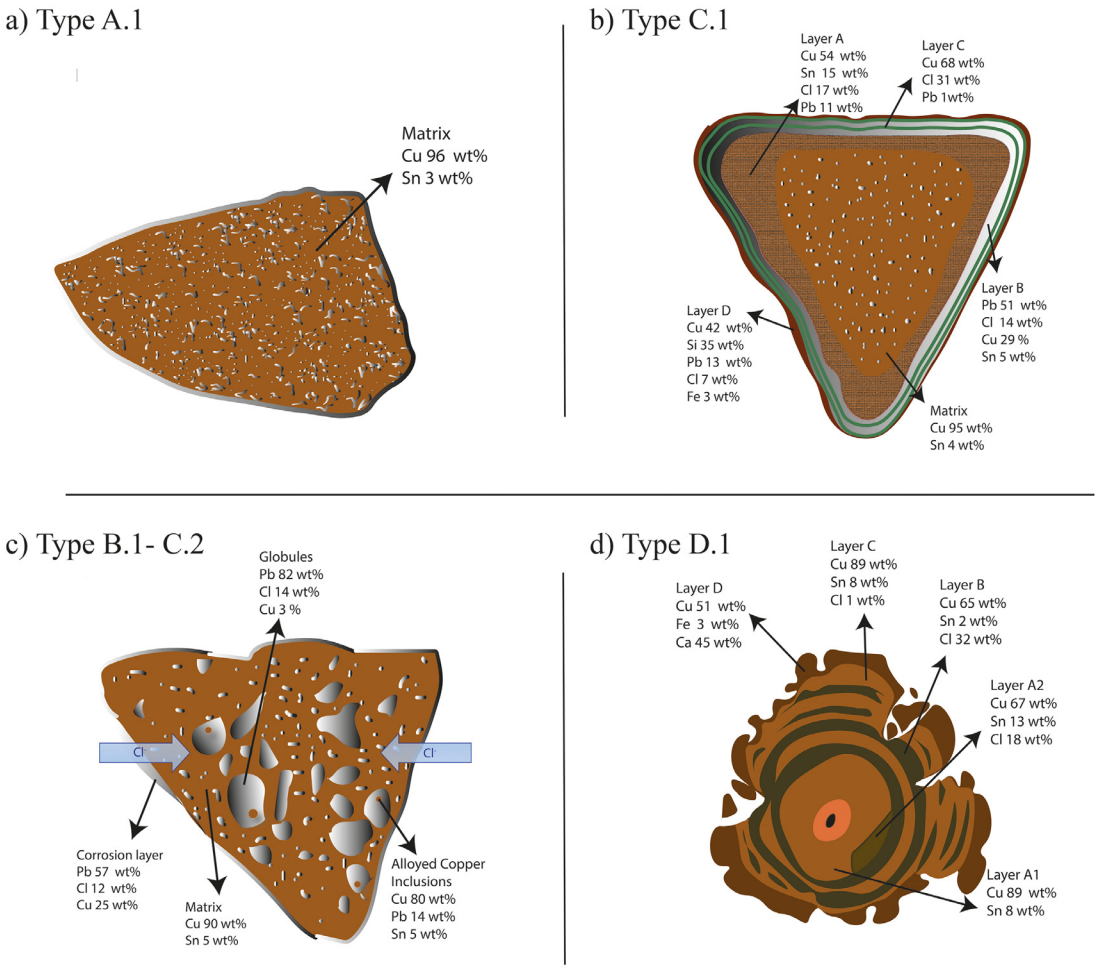

Fig. 4. Schematic representation of the corrosive structure of the arrowheads: (a) A.1 (b) C.1, (c) B.1- C.2, (d) D.1. All values reported here represent the approximate average composition of each layer in four different typologies of alloys (see Table 2).

were also used by the Phoenicians in the Siege of Motya and were imported from Sardinia or other countries.

On the other hand, arrowheads with a simpler conical shape (Type D.1) are made up of alloys without Pb. This kind of arrowhead appears to be a Motyan prototype and has been documented in Himera and Segesta (Sicily), but has never been recovered in other Mediterranean settlements. This would suggest that the Phoenicians produced good quality weapons, consisting of a harder type of binary alloy with high Sn content. The Liesegang rings resulting from the corrosion process could be related to the distinctive manufacture of this arrowhead, which involved wrapping a metal foil on itself to achieve its conical shape.

Conclusions

This work has investigated the key role of the chemical composition of arrowheads used during the Siege of Motya and how corrosion has affected their mechanical properties. The results of this study support the following main conclusions:

- EDS and EMPA data have highlighted that Sn content played a key role in the corrosion process of Pb-free bronze in conical arrowheads (Type D.1). In fact, Sn-rich streaks are interposed between Liesegang rings, leading to the formation of $Cu_2(OH)_3Cl$ through redox reactions between intermediate Sn- and Cu-chlorides.
- The arrowheads with more accessory elements such as wings and barbs and a higher Pb content formed large Pb-globules (Type B.1 and C.2) or Pb- fine dispersion in the grain boundaries (Type A.1 and C.1).
- XRPD results have suggested that bronze disease affected all samples characterized by the presence of Pb-chlorides in the alloy interface. In addition, a significant stratification of copper trihydroxychlorides and mixed salts of Cu and Pb (*i.e.*, pseudoboleite) formed in alloys with smaller Pb microdomains, whereas in alloys with large Pb globules lead salts (*i.e.*, penfieldite and cotunnite) predominated.
- The harder Cu-Sn-binary alloy with high Sn content, used for the production of conical arrowheads in Motya, suggests that the Motyan people defended themselves with good quality weapons in spite of their tragic defeat. Meanwhile, the pyramidal and lanceolate arrowheads ascribed to the troops of Dionysius I of Syracuse were made of a modern type of ternary alloy with lower mechanical resistance due to the presence of Pb.

Acknowledgements

The arrowheads have been uncovered by the Sapienza Archaeological Expedition to Motya thanks to the fruitful cooperation with the Superintendency of Trapani of the Sicilian Region, and the G. Whitaker Foundation, Palermo.

This research work is a product of the PRIN 2017 Project: “People of the Middle Sea. Innovation and integration in ancient Mediterranean (1600-500 BC)” [B.2. Innovative metallurgy], funded by the Italian Ministry of Education, University and Research.

Financial support was also provided by Sapienza University of Rome (Great Excavation Funds; Ateneo funding, 2016, 2018). PhD grants of the Department of Earth Sciences, Sapienza University of Rome, are gratefully acknowledged. The authors thank Dr. Katie Farrar for English Editing.

Supplementary materials

Supplementary material associated with this article can be found, in the online version, at doi:10.1016/j.culher.2021.10.001.

References

[1] D. Ashkenazi, How can fracture mechanics and failure analysis assist in solving mysteries of ancient metal artifacts? Archaeol. Anthropol. Sci. 12 (2020), doi:10.1007/s12520-019-00970-w.
[2] M. Bernabale, L. Nigro, D. Montanari, A.M. Niveau-de-villedary, C. De Vito, Materials Characterization Microstructure and chemical composition of a Sardinian bronze axe of the Iron Age from Motya (Sicily, Italy), Mater. Charact. 158 (2019), doi:10.1016/j.matchar.2019.109957.
[3] D.J. Chakrabarti, D.E. Laughlin, The Cu– Pb (Copper-Lead) system, Bull. Alloy Phase Diag. 5 (1984) 503–510.
[4] T. Chang, G. Herting, S. Goidanich, J.M. Sánchez Amaya, M.A. Arenas, N. Le Bozec, Y. Jin, C. Leygraf, I. Odnevall Wallinder, The role of Sn on the long-term atmospheric corrosion of binary Cu-Sn bronze alloys in architecture, Corros. Sci. 149 (2019) 54–67, doi:10.1016/j.corsci.2019.01.002.
[5] T. Chang, A. Maltseva, P. Volovitch, I. Odnevall Wallinder, C. Leygraf, A mechanistic study of stratified patina evolution on Sn-bronze in chloride-rich atmospheres, Corros. Sci. 166 (2020) 108477, doi:10.1016/j.corsci.2020.108477.
[6] M.F. Charlton, P. Crew, T. Rehren, S.J. Shennan, Explaining the evolution of ironmaking recipes – an example from northwest Wales, J. Anthropol. Archaeol. 29 (2010) 352–367, doi:10.1016/j.jaa.2010.05.001.
[7] S. Chattopadhyay, S. Srikanth, The Cu-Pb-Sn (copper-lead-tin) system, J. Phase Equilibria 15 (1994) 553–557, doi:10.1007/BF02649416.
[8] I. Constantinides, A. Adriaens, F. Adams, Surface characterization of artificial corrosion layers on copper alloy reference materials, Appl. Surf. Sci. 189 (2002) 90–101, doi:10.1016/S0169-4332(02)00005-3.
[9] F.J.R. De Oliveira, D.C.B. Lago, L.F. Senna, L.R.M. de Miranda, E. D'Elia, Study of patina formation on bronze specimens, Mater. Chem. Phys. 115 (2009) 761–770, doi:10.1016/j.matchemphys.2009.02.035.
[10] M. Di Fazio, A.C. Felici, F. Catalli, C. De Vito, Microstructure and chemical composition of Roman orichalcum coins emitted after the monetary reform of Augustus (23 B.C.), Sci. Rep. 9 (2019) 1–11, doi:10.1038/s41598-019-48941-4.
[11] F. Di Turo, F. Coletti, C. De Vito, Investigations on alloy-burial environment interaction of archaeological bronze coins, Microchem. J. 157 (2020) 104882, doi:10.1016/j.microc.2020.104882.
[12] A. Doménech-Carbó, M. Doménech-Carbó, I. Martínez-Lázaro, Electrochemical identification of bronze corrosion products in archaeological artefacts. A case study, Microchim. Acta 162 (2008) 351–359, doi:10.1007/s00604-007-0839-3.
[13] M.T. Doménech-Carbó, F. Di Turo,, N. Montoya, F. Catalli, A. Doménech-Carbó, C De Vito, FIB-FESEM and EMPA results on Antoninianus silver coins for manufacturing and corrosion processes, Sci. Rep. 8 (1) (2018) 1–12.
[14] R. Edwards, R.D. Gillard, P.A. Williams, A.M. Pollard, Studies of secondary mineral formation in the PbO-H 2 O-HC1 system, Mineral. Mag. 56 (1992) 53–65, doi:10.1180/minmag.1992.056.382.07.
[15] L. Fabrizi, F. Di Turo, L. Medeghini, M. Di Fazio, F. Catalli, C. De Vito, The application of non-destructive techniques for the study of corrosion patinas of ten Roman silver coins: the case of the medieval Grosso Romanino, Microchem. J. 145 (2019) 419–427, doi:10.1016/j.microc.2018.10.056.
[16] I.T.E. Fonseca, R. Picciochi, M.H. Mendonça, A.C. Ramos, The atmospheric corrosion of copper at two sites in Portugal: a comparative study, Corros. Sci. 46 (2004) 547–561, doi:10.1016/S0010-938X(03)00176-8.
[17] A.R. Giumlia-Mair, The composition of copper-based small finds from a west Phoenician settlement site and from Nimrud compared with that of contemporary Mediterranean small finds, Archaeometry 34 (1992) 107–119.
[18] J. Goñi, C. Guillemin, R. Perrimond-Tronchet, Description d'espèces minérales néogènes formées sur des jas d'ancres romaines immergées, Bull. Minér. 77 (1954) 474–478.
[19] M.J. Hughes, J.P. Northover, B.E.P. Staniaszek, Problems in the analysis of leaded bronze alloys in ancient artefacts, Oxf. J. Archaeol. 1 (1982) 359–364, doi:10.1111/j.1468-0092.1982.tb00320.x.
[20] M.J. Hutchison, J.R. Scully, Patina enrichment with SnO 2 and its effect on soluble Cu cation release and passivity of high-purity Cu-Sn bronze in artificial perspiration, Electrochim. Acta 283 (2018) 806–817, doi:10.1016/j.electacta.2018.06.125.
[21] G.M. Ingo, C. Riccucci, G. Guida, M. Pascucci, C. Giuliani, E. Messina, G. Fierro, G. Di Carlo, Micro-chemical investigation of corrosion products naturally grown on archaeological Cu-based artefacts retrieved from the Mediterranean sea, Appl. Surf. Sci. 470 (2019) 695–706, doi:10.1016/j.apsusc.2018.11.144.
[22] S. Klein, Iron Age Leaded Tin Bronzes from Khirbet Edh-Dharih, Jordan, 1999, pp. 1075–1082.
[23] C. Leygraf, T. Chang, G. Herting, I.O. Wallinder, The origin and evolution of copper patina colour, Corros Sci 157 (2019) 337–346.
[24] L. Nigro, Before the Greeks: the earliest phoenician settlement in Motya—recent discoveries by Rome 'La Sapienza'Expedition, Vicin. Oriente 17 (2013) 39–74.
[25] L. Nigro, D. Montanari, F.M.-M. Bernabale, C. De Vito, A Sardinian early 1st millennium BC bronze axe from Motya, Vicin. Oriente. 24 (2020) 57–74.
[26] L. Nigro, G. Rossoni, La Sapienza" a Mozia, Quarant'anni di Ricerca Archeologica (1964-2004) (2004).
[27] R.M. Organ, Aspects of Bronze patina and its treatment, Stud. Conserv. 8 (1) (2006), doi:10.2307/1505097.
[28] O. Oudbashi, Multianalytical study of corrosion layers in some archaeological copper alloy artefacts, Surf. Interface Anal. 47 (2015) 1133–1147, doi:10.1002/sia.5865.
[29] O. Oudbashi, S.M. Emami, H. Ahmadi, P. Davami, Micro-stratigraphical investigation on corrosion layers in ancient Bronze artefacts by scanning electron microscopy energy dispersive spectrometry and optical microscopy, Herit. Sci. 1 (2013) 1–10, doi:10.1186/2050-7445-1-21.
[30] M. Quaranta, E. Catelli, S. Prati, G. Sciutto, R. Mazzeo, Chinese archaeological artefacts: microstructure and corrosion behaviour of high-leaded bronzes, J. Cult. Herit. 15 (2014) 283–291, doi:10.1016/j.culher.2013.07.007.
[31] L. Robbiola, J.-M. Blengino, C. Fiaud, Morphology and mechanisms of formation of natural patinas on archaeological Cu–Sn alloys, Corros. Sci. 40 (1998) 2083–2111.
[32] L. Robbiola, C. Fiaud, A. Harch, Characterisation of passive layers of bronze patinas (Cu-Sn alloys) in relation with the tin content of the alloy, in: Eur. Symp. Modif. Passiv. Film. Paris 15-17 Feb. 1993, 1993, pp. 150–154.
[33] L. Robbiola, L. Hurtel, Standard nature of the passive layers of buried archaeological bronze - the example of two Roman half-length portraits, Met. 95 Int. Conf. Met. Conserv. - MacLEod I., Pennec S. Robbiola L. Ed., 1997.
[34] I. Sandu, O. Mircea, A.V. Sandu, V. Vasilache, I.G. Sandu, Study of the Liesegang chemical effects in antique bronze artefacts during their stay within an archaeological site, Rev. Chim. (2014) 65.
[35] I. Sandu, M. Quaranta, C. Bejinariu, I.G. Sandu, D. Luca, A.V. Sandu, Study on the specific effects of corrosion processes on ancient bronze artefacts. The annals of "Dunarea de Jos" University of Galati. Fascicle IX, Metall. Mater. Sci. 30 (1) (2007) 64–73.
[36] I. Sandu, N. Ursulescu, I.G. Sandu, O. Bounegru, I.C.A. Sandu, A. Alexandru, Pedological stratification effect of corrosion and contamination products on Byzantine bronze artefacts, Corros. Eng. Sci. Technol. 43 (2008) 256–266, doi:10.1179/174327807x234688.
[37] I.G. Sandu, F.A. Tencariu, D.M. Vornicu, A.V. Sandu, A. Vornicu, V. Vasilache, I. Sandu, Establishing the archaeo-metallurgic ornamentation process of an axe from the bronze age by OM, SEM-EDX, and Micro-FTIR, Microsc. Res. Tech. 77 (11) (2014) 918–927, doi:10.1002/jemt.22416.
[38] D.A. Scott, Periodic corrosion phenomena in bronze antiquities, Stud. Conserv. 30 (49) (2006), doi:10.2307/1506088.
[39] M. Serghini-idrissi, M.C. Bernard, F.Z. Harrif, S. Joiret, K. Rahmouni, A. Srhiri, H. Takenouti, V. Vivier, M. Ziani, Electrochemical and spectroscopic characterizations of patinas formed on an archaeological bronze coin, Electrochim. Act 50 (2005) 4699–4709, doi:10.1016/j.electacta.2005.01.050.
[40] D. Siculus, C.H. Oldfather, C.L. Sherman, B.C. Welles, R.M. Geer, F.R. Walton, in: The Library of History (Book XIV, Harvard University Press, Cambridge, Mass, 2006, pp. 40–78.
[41] N. Souissi, L. Bousselmi, S. Khosrof, E. Triki, Electrochemical behaviour of an archaeological bronze alloy in various aqueous media: new method for understanding artifacts preservation, Mater. Corros. 54 (2003) 318–325, doi:10.1002/maco.200390071.
[42] A. Termini, Le punte di freccia in bronzo nella Sicilia punica, A. Spanò Giammellaro (2005) 653–665.
[43] V. Tusa, Le armi dei corredi tombali della necropoli arcaica di Mozia", Vicin. Oriente 16 (2012) 131–150.
[44] P. Valério, R.J.C. Silva, M.F. Araújo, A.M.M. Soares, L. Barros, A multianalytical approach to study the Phoenician bronze technology in the Iberian Peninsula-A view from Quinta do Almaraz, Mater. Charact. 67 (2012) 74–82, doi:10.1016/j.matchar.2012.02.020.
[45] X. Zhang, An unusual corrosion product, pyromorphite, from a Bronze An: a technical note, Stud. Conserv. 47 (76) (2008), doi:10.2307/1506836.
[46] X. Zhang, I. Odnevall Wallinder, C. Leygraf, Mechanistic studies of corrosion product flaking on copper and copper-based alloys in marine environments, Corros. Sci. 85 (2014) 15–25, doi:10.1016/j.corsci.2014.03.028.
[47] K.M. Zohdy, M.M. Sadawy, M. Ghanem, Corrosion behavior of leaded-bronze alloys in sea water, Mater. Chem. Phys. 147 (2014) 878–883, doi:10.1016/j.matchemphys.2014.06.033.